Biometry for IOL Power Prediction

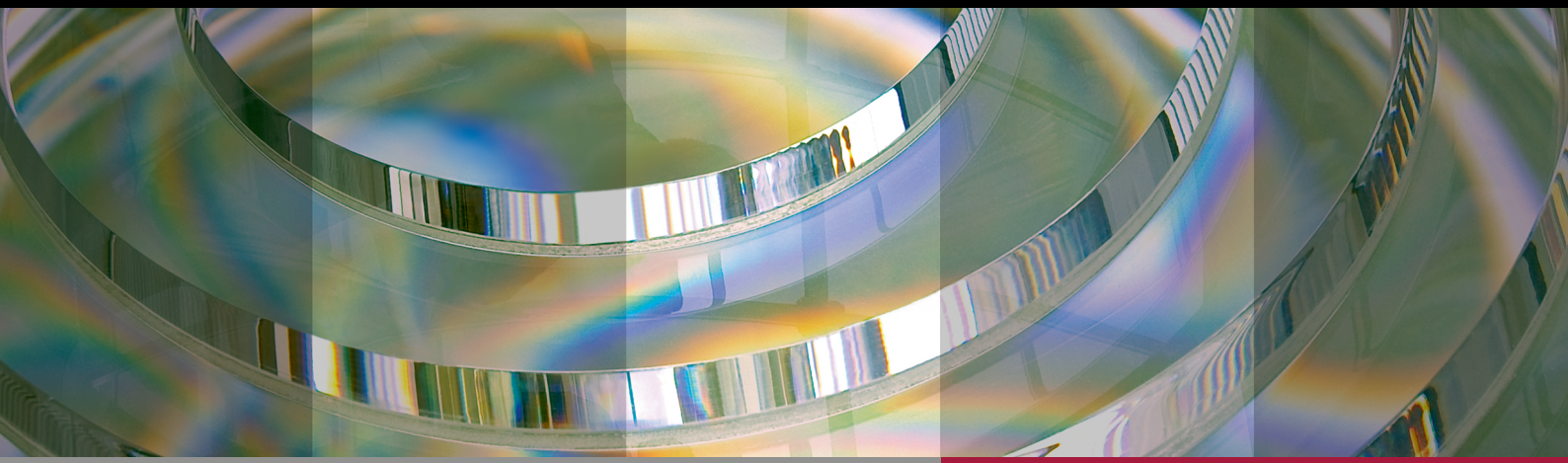

ANTERION®

HEIDELBERG ENGINEERING

ACADEMY

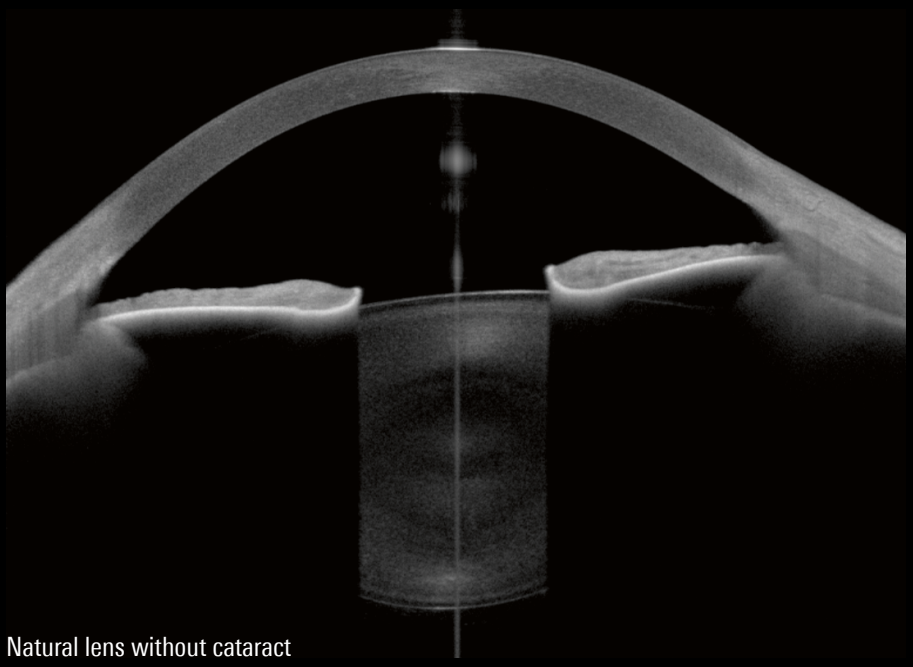

Natural lens without cataract

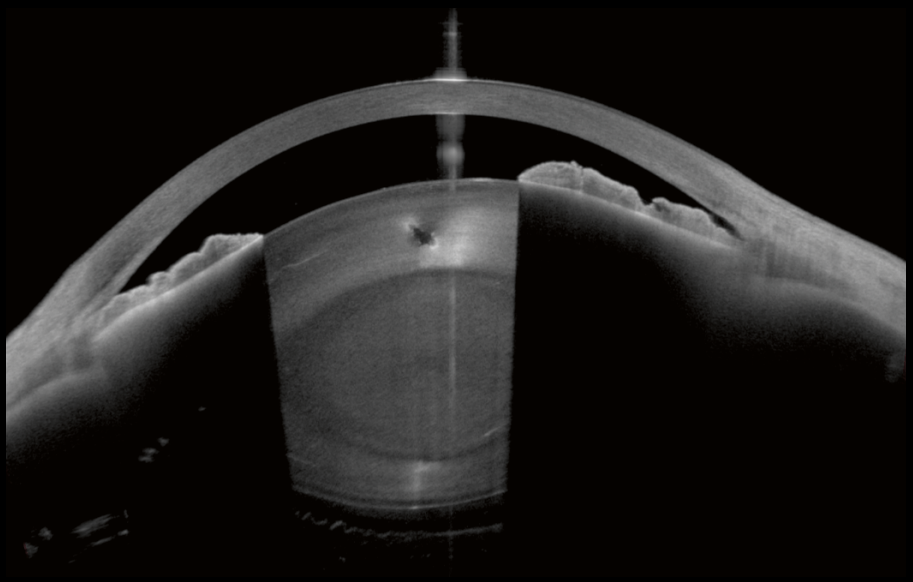

Dense cataract

Image courtesy: Tobias Duncker, MD, Halle, Germany

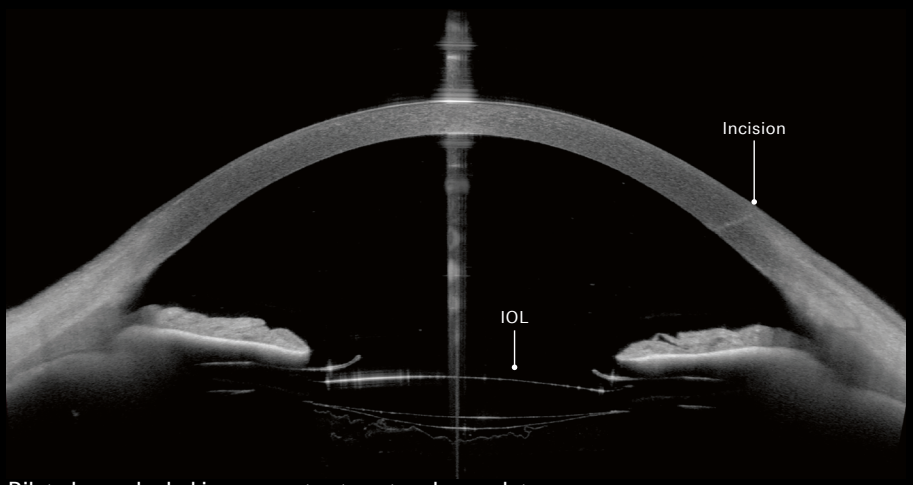

Dilated pseudophakic eye, post cataract and capsulotomy

Image courtesy: Ulrich Kellner, MD, Siegburg, Germany

Table of Contents

This tutorial is not intended as a diagnostic guide and is not a substitute for clinical experience and assessment.

When diagnosing and treating patients, each clinician must analyze and interpret all available data and make individual clinical decisions based on their clinical assessment and experience.

The diagnosis is the responsibility of the physician.

Biometry OU Overview

OU
Biometry OU

IF CORNEA APP AND CATARACT APP ARE AVAILABLE

All corneal maps are automatically provided within the Cataract App after the examination. If a follow-up measurement on corneal maps is planned, perform an additional examination with the Cornea App.

1 Selected app with number of acquisitions.

3 Menu bar to open application-specific views.

4 Camera image with overlay and views of the OCT section image, the anterior axial curvature or the total corneal power map. When moving the mouse over the map, the exact value at that point is displayed.

7 **Default settings** to configure general and app-specific (default) settings as a user with keyuser rights.

8 **More** section:

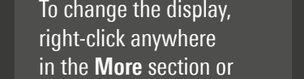

Basics tab with cornea parameters and **Premium IOL** tab with parameters for IOL selection and power prediction.

The **OD-OS Difference** column highlights differences between both eyes, as the right and left eye are similar in most patients.

UNITS

Switch unit to mm/D

Parameters and most curvature maps are available both in power [D] and radius [mm]. To change the display, right-click anywhere in the **More** section or in the map and select the desired unit of measurement.

Fig. 1: Biometry OU Overview.

Checking Examination Quality

EXAMINATION QUALITY

Make sure that the ANTERION examination is the first step within your examination workflow in preparation for cataract surgery.

1 Click **Info**.

2 Verify that the correct eye status has been selected and correct it, if necessary (p.15).

3 Check that the fixation light focus is appropriate.

OD-OS DIFFERENCE

Differences between OD and OS, e.g., different eye lengths or corneal parameters, may thus be interpreted more conclusively.

4 Check that the acquisition quality parameters are marked as ✓ Pass or ✓ Borderline.

ACQUISITION QUALITY PARAMETERS

If one or more of the acquisition quality parameters are marked as ✗ Fail, decide on a case-by-case basis if the acquired data should be assessed. It is recommended to repeat the examination, as the results may be inaccurate.

5 Check segmentations of anatomic boundaries at vertex and edit them, if necessary (p.13).

6 Review axial length value and graph. Enter or edit them manually, if necessary (p.15).

*Fig. 2: Checking examination quality with the help of the **Info** tab.*

The following chapter uses a normal eye with high astigmatism to provide an overview of corneal maps relevant for IOL power prediction and their schematic illustrations as well as biometry parameters and their observed ranges reported in literature.

The reported ranges were determined by meta-analysis including the referenced publications. They include values that would be expected for typical measurements in healthy patients (95 % quantiles).

Please note that these values are not suitable for the definition of normal ranges for diagnostic purposes.

CORNEAL MAP AVAILABILITY

While the **anterior axial curvature** and **total corneal power** maps are also available with the Cataract App license, the other maps are only available with the Cornea App license.

2.1 Anterior Axial Curvature

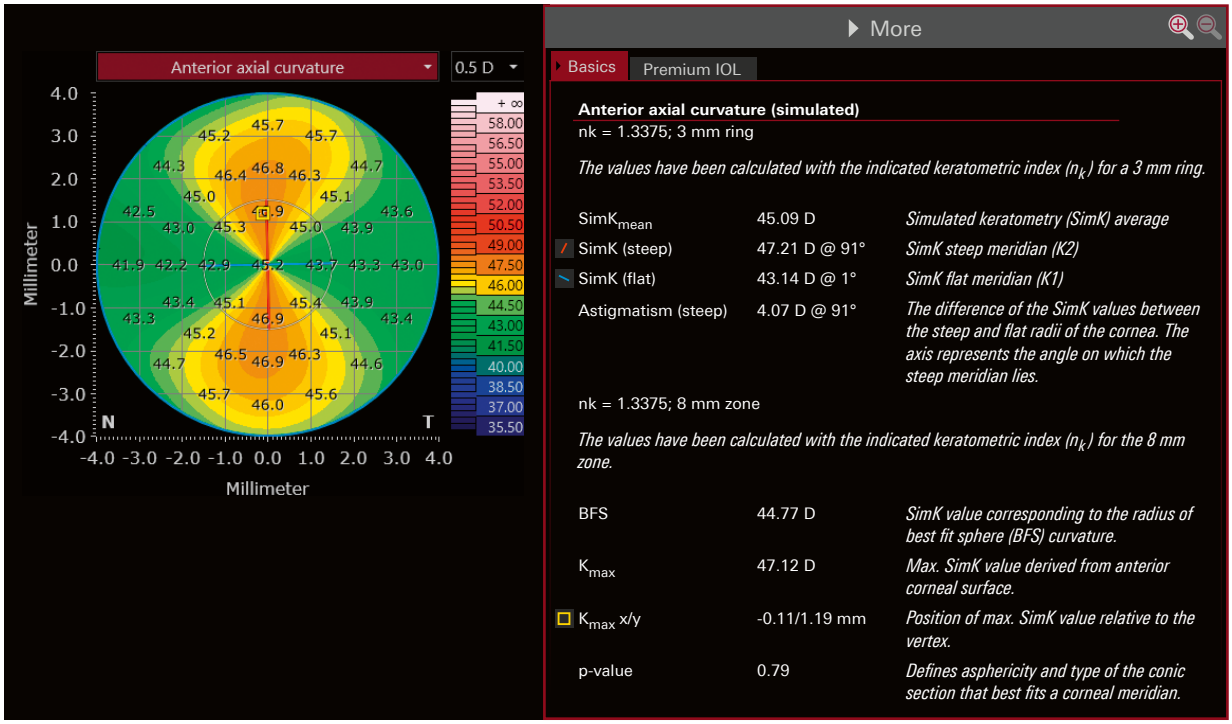

Fig. 3 Anterior axial curvature: Map and parameters.

The anterior axial curvature map can be displayed in either radius [mm] or power [D]. The radii are derived from OCT data and the conversion of curvature [mm] to SimK [D] is calculated according to the laws of Gaussian optics using the keratometric index of 1.3375. The refractive effect and the posterior corneal surface radii are not considered.

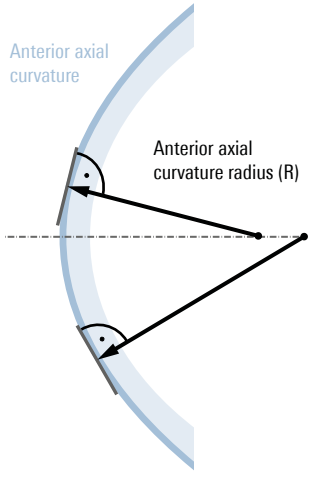

Fig. 4 Anterior axial curvature: Schematic illustration.

REPORTED RANGES

Anterior Axial Curvature (3 mm Ring)

R_{mean} [1–7]	8.02 – 7.57 mm
$SimK_{mean}$ [1–7]	42.1 – 44.6 D

ECCENTRICITY / ASPHERICITY / SHAPE FACTOR

The degree of the cornea flattening towards the periphery can be described by:

- **p-value:** Sphere (p = 1), prolate (1 > p > 0) or oblate ellipsoid (p > 1),
- **Q-value:** Sphere (Q = 0), prolate (-1 < Q < 0) or oblate ellipsoid (Q > 0), or
- **E-value:** Sphere (E = 0), prolate (0 < E < 1) or oblate ellipsoid (E < 0).

The value to be displayed as default can be changed in the default settings.

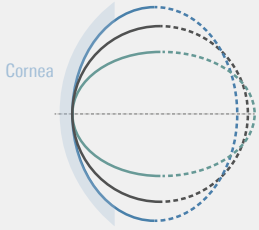

Fig. 5 Sphere, prolate and oblate ellipse.

2.2 Posterior Axial Curvature

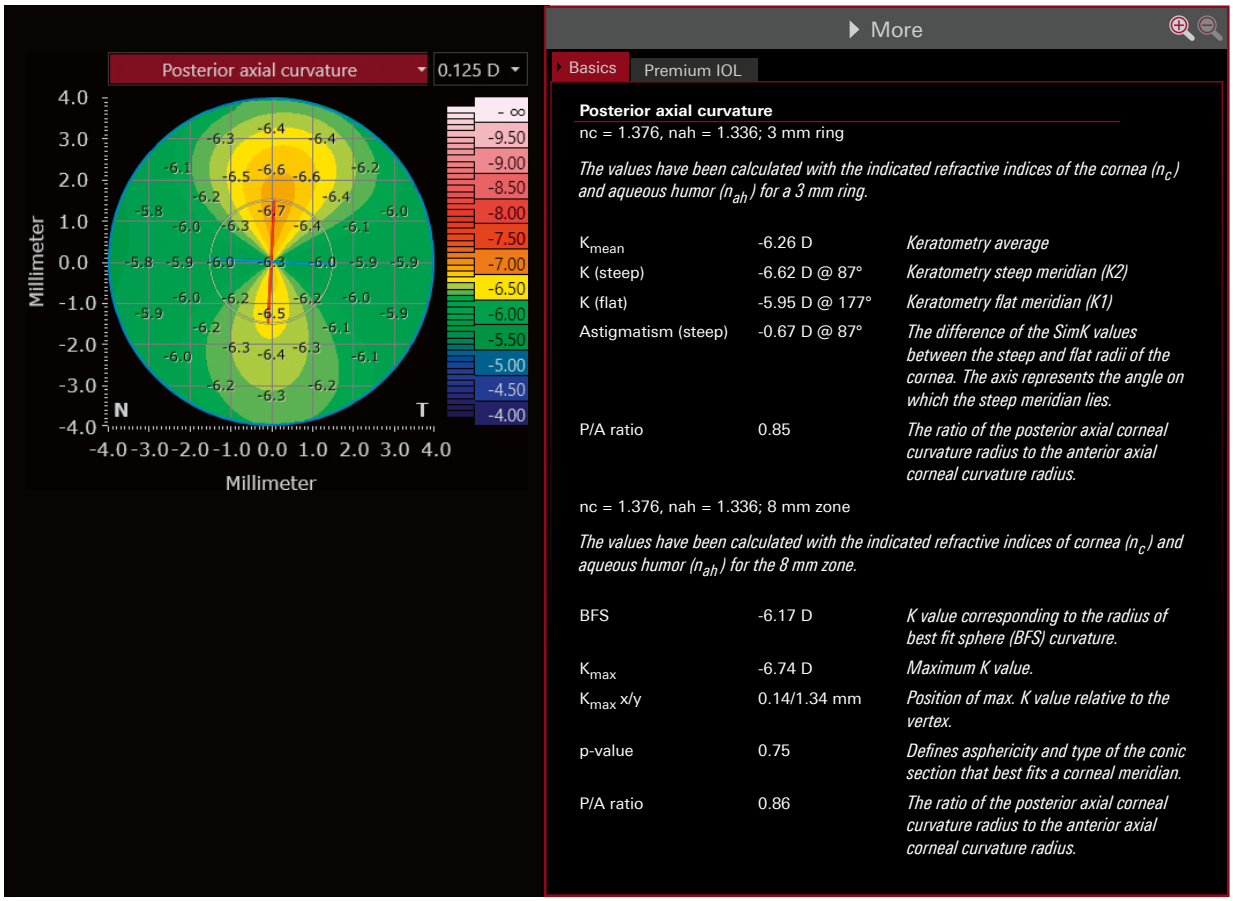

Fig. 6 Posterior axial curvature: Map and parameters.

The posterior axial curvature map can be displayed in either radius [mm] or power [D]. The radii are derived from OCT data and the conversion of curvature [mm] to K [D] is calculated according to the laws of Gaussian optics using the refractive indices of the cornea (n_c) and the aqueous humor (n_{ah}).

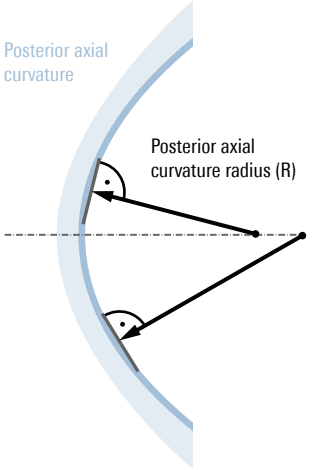

Fig. 7 Posterior Axial Curvature: Schematic illustration.

REPORTED RANGES

Posterior Axial Curvature (3 mm Ring)

K_{mean} [1–10]	-5.6 – -6.6 D
P/A ratio [20]	0.82 – 0.86

2.3 Astigmatism (Steep)

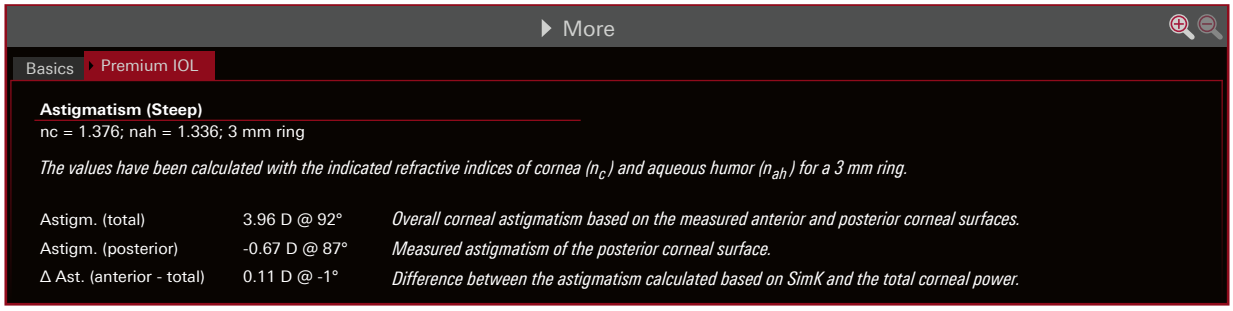

Fig. 8 Astigmatism (Steep): Parameters.

2.4 Total Corneal Power

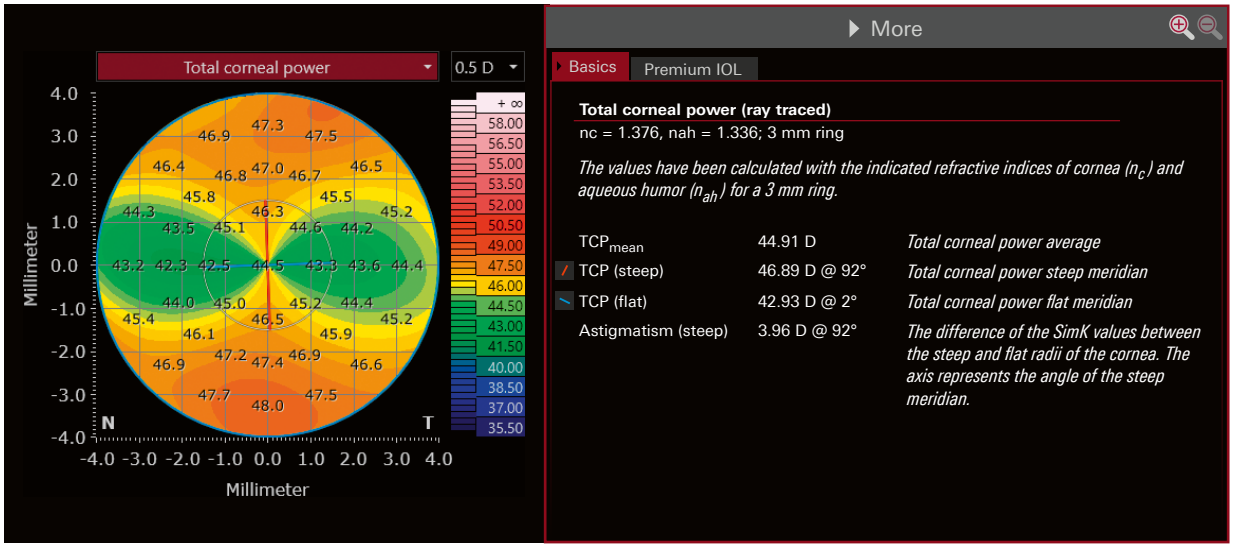

Fig. 9 Total corneal power: Map and parameters.

The total corneal power (TCP) map shows the TCP calculated using ray tracing. This takes into account the refraction of parallel incident light beams (assumption) at the anterior and posterior corneal surfaces as a function of their refractive indices. Each point on the map correlates to a resulting focal length, from which the corresponding refractive power is calculated.

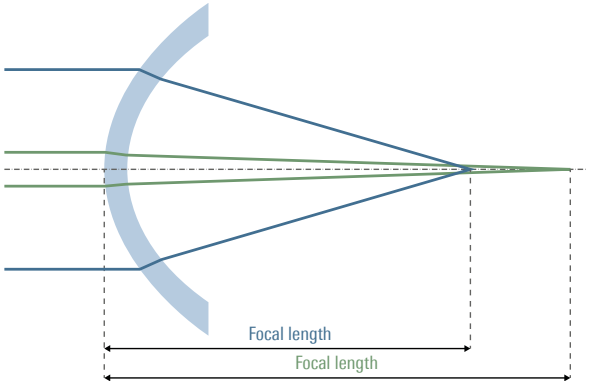

Fig. 10 Total corneal power: Schematic illustration.

2.5 Total Corneal Wavefront

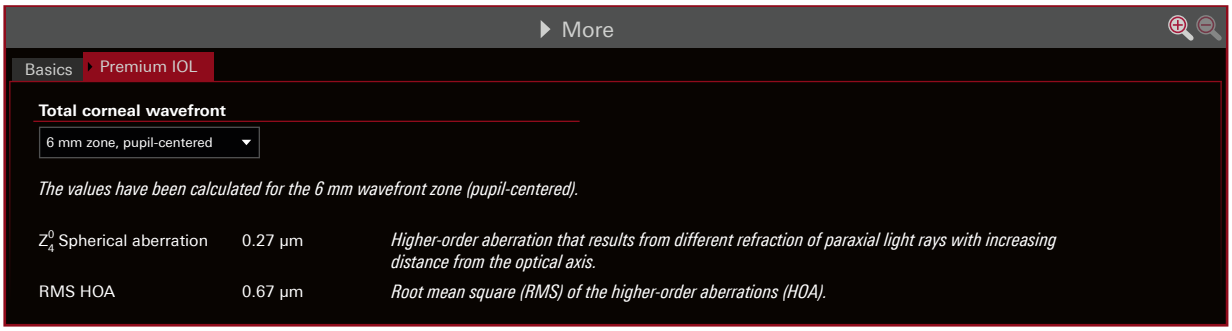

Fig. 11 Total corneal wavefront: Parameters.

REPORTED RANGES

Total Corneal Wavefront (6 mm)

Z_4^0 Spherical aberration [21]	0.25 – 0.27 µm
RMS HOA [21]	0.45 – 0.48 µm

ZONE SIZE

6 mm zone, pupil-centered

Choose the zone size used for the total corneal wavefront from 3–8 mm pupil-centered via the drop-down menu. In the default settings, you can set a specific size as default.

2.6 Pachymetry

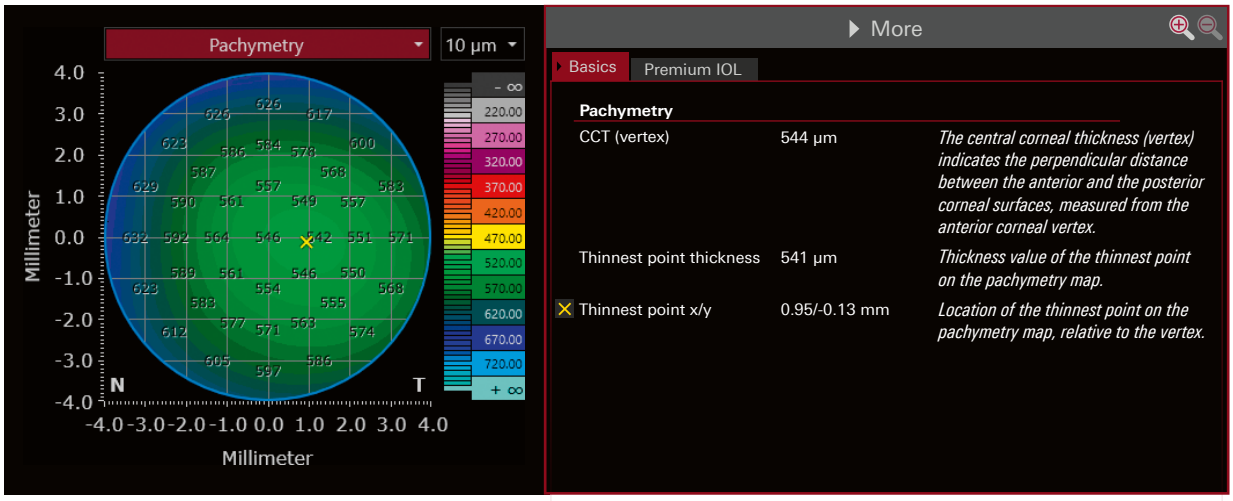

Fig. 12 Pachymetry: Map and parameters.

The pachymetry map shows the thickness of the cornea over an 8 mm map along a plane perpendicular to the anterior corneal surface. The warmer the shown colors are, the thinner is the cornea. The thinnest point can be displayed by selecting the corresponding overlay **Thinnest point x/y** within the **Pachymetry** section (✕).

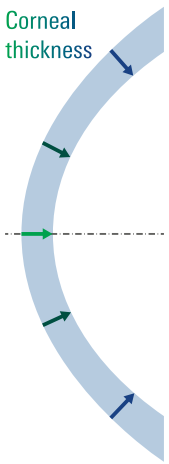

Fig. 13 Pachymetry: Schematic illustration.

REPORTED RANGES

Pachymetry

CCT (vertex) [1–4, 6–15]	474 – 608 µm

2.7 Anterior Segment

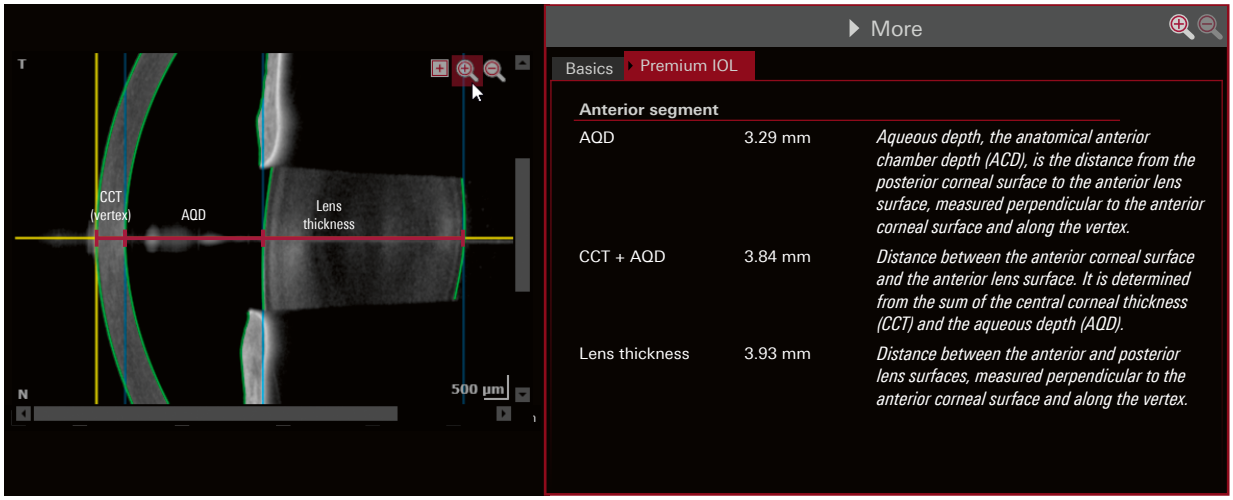

Fig. 14 Anterior Segment: Parameters.

REPORTED RANGES

Anterior Segment

AQD (ACD) [4, 15–19]	2.11 – 3.91 mm
Lens thickness [4, 12–15, 22]	3.43 – 4.77 mm

2.8 Pupil & White-to-White (WTW)

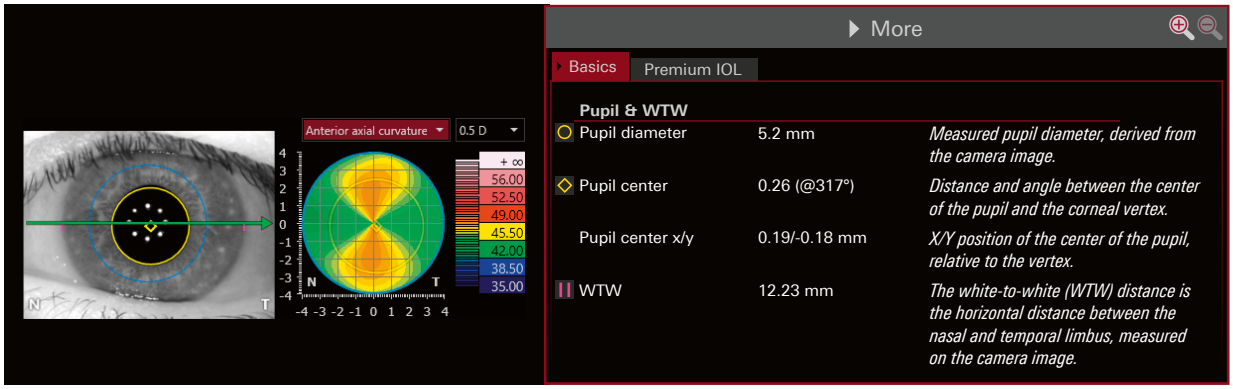

Fig. 15 Pupil & WTW (white-to-white): Overlays and parameters.

REPORTED RANGES

White-to-white

WTW [2–4, 12–14, 22–25]	11.0 – 12.8 mm

Editing Anatomic Boundaries

INCORRECT ANATOMIC BOUNDARIES

If the boundaries of the anterior corneal surface were not correctly detected, reexamine the patient.

If the boundaries of the posterior corneal surface, anterior lens surface, and/or posterior lens surface were not correctly detected, manually adjust the corresponding boundaries or consider retaking an examination.

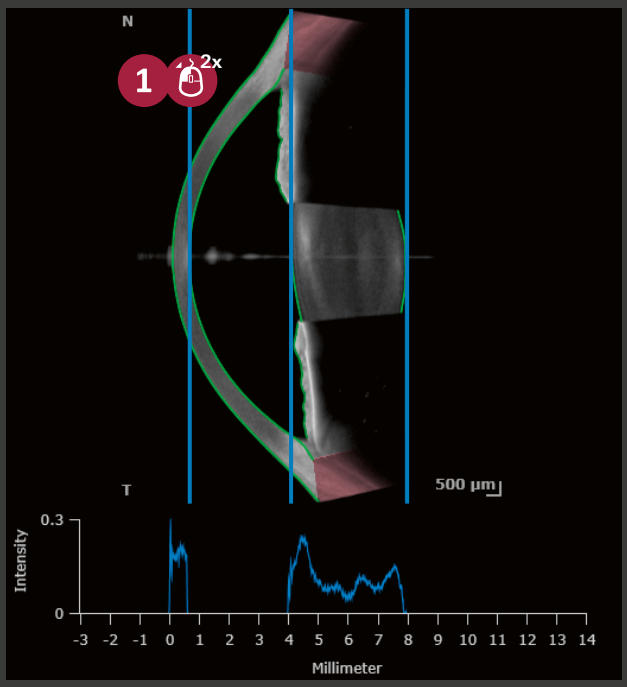

*Fig. 16: Anatomic boundaries in the **Biometry OU** view.*

1. Double-click one of the blue vertical lines on the OCT section image to edit the anatomic boundaries. The segmentation editor opens.
2. Drag and drop the vertical lines of the posterior corneal surface, anterior and/or posterior lens surface to the desired position.
3. Click **Save and close** to confirm the changes.
4. If you want to reset your changes to the default image, click **Restore all**.

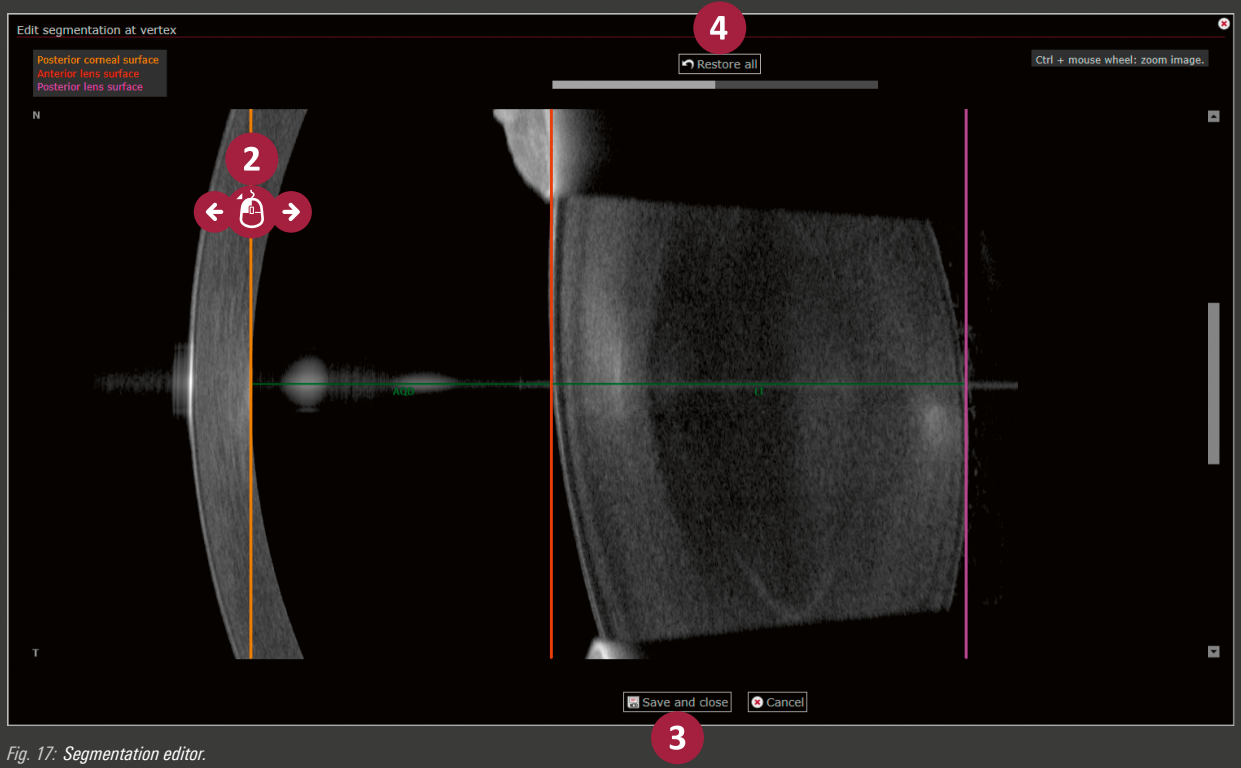

Fig. 17: Segmentation editor.

2.9 Axial Length

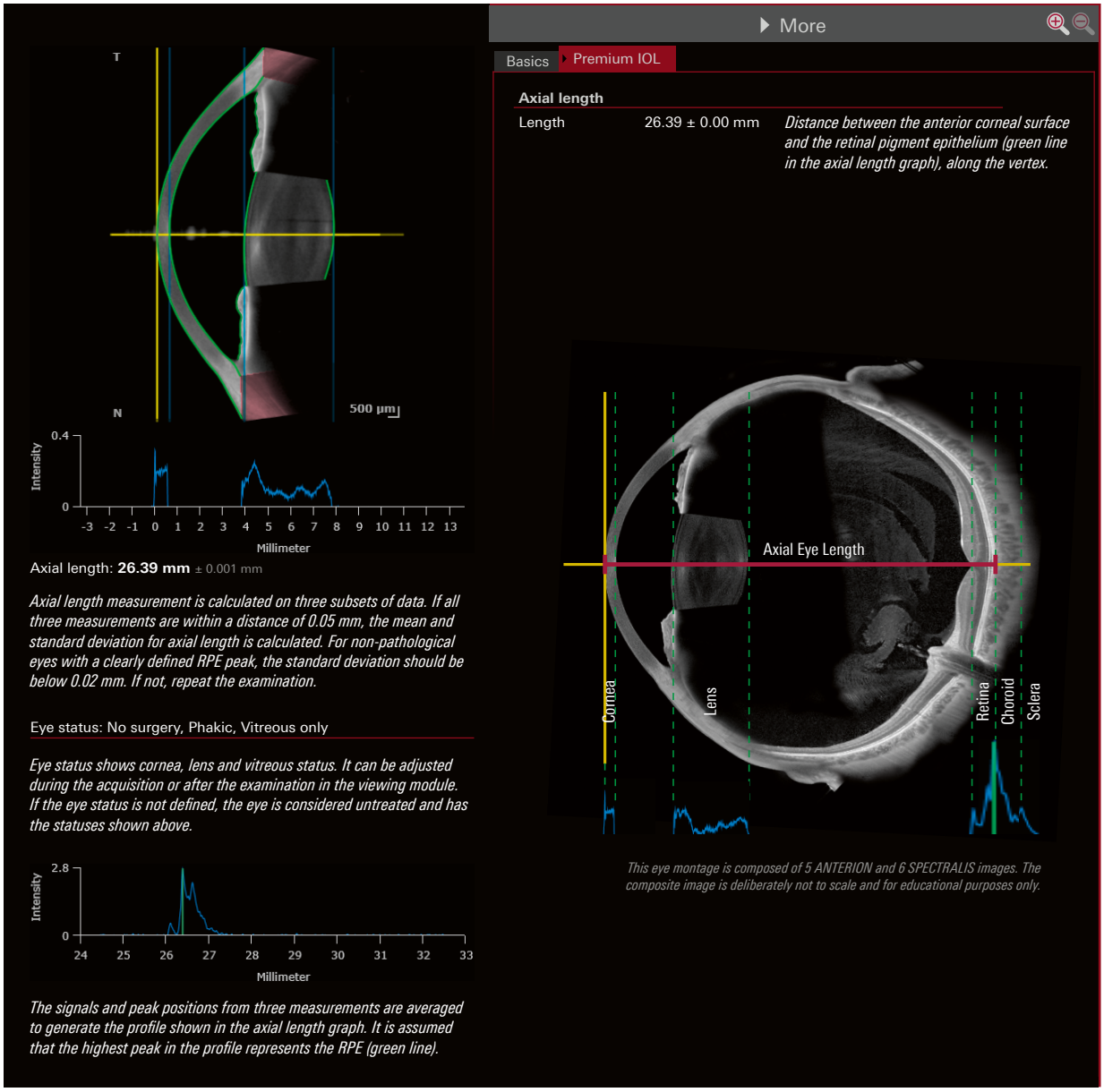

Fig. 18 Axial Length: Parameter and section with eye status and intensity graphs.

REPORTED RANGES

Axial Length

Length [4, 10–15, 22]	21.5 – 26.4 mm

Axial Length Values

CHECKING AXIAL LENGTH VALUES

Fig. 19: Axial length measurement with axial length value and graph.

1. Check axial length values of both eyes. If they differ significantly, check whether the measured values are plausible in relation to the set fixation light focus and refraction.
2. Check if the standard deviation is < 0.02 mm. If not, repeat the examination and ensure a stable fixation of the patient's eye.
3. Check the axial length graph for plausibility and correct it, if needed (p.16).

NO AXIAL LENGTH GRAPH IS DISPLAYED

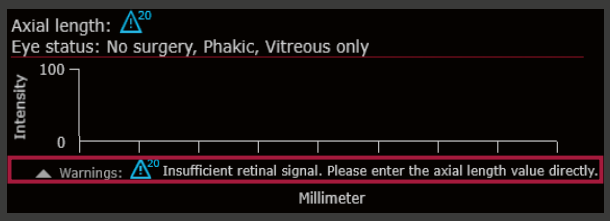

Fig. 20: Axial length measurement without axial length value and graph.

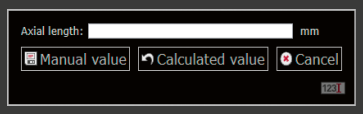

Fig. 21: Manual axial length.

1. If no axial length value is displayed, e.g., if certain eye statuses are selected, the fixation light focus was not adjusted accordingly, or if the retinal signal is reduced due to opacities such as hemorrhage or asteroid hyalosis, repeat the examination.
2. If the measurement still fails, it is possible to enter the eye length measured with ultrasound manually. Click **Axial length**, enter the value and confirm by clicking **Manual value**.

Eye Status

Check if the eye status is correct and edit it if necessary:

1. Click **Eye status.**
2. Select the status from the drop-down list.
3. Confirm by clicking **Save and close.**

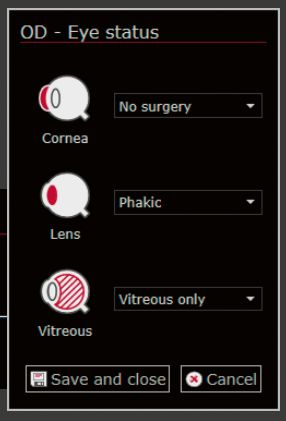

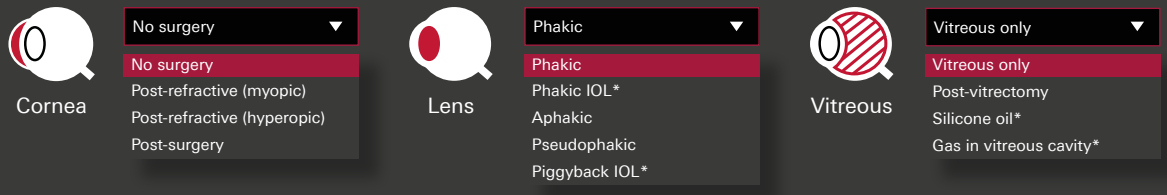

Fig. 22: Editing eye status.

* No axial length value displayed.

Axial Length Graph

The reflected signals from different retinal structures, e.g., internal limiting membrane (ILM) and retinal pigment epithelium (RPE), but also the choroid and sclera, result in an axial length graph. The higher the structure reflects within or behind the retina (choroid, sclera), the higher is the resulting intensity in the graph.

APPEARANCE OF THE AXIAL LENGTH GRAPH

Where the laser beam first hits the retina, the ILM is to be assumed. The highest detected retinal peak is assigned to the RPE, as this represents the highest reflective structure within a healthy retina.
The axial length graph is thus characterized by an initial small to moderate peak (ILM) to the highest peak (RPE).

However, axial length graph appearances and intensities may vary depending on opacities in the anterior segment, individual characteristics and conditions of the retinal structures (especially ILM and RPE), choroid/sclera signal, fixation light focus setting and fixation.

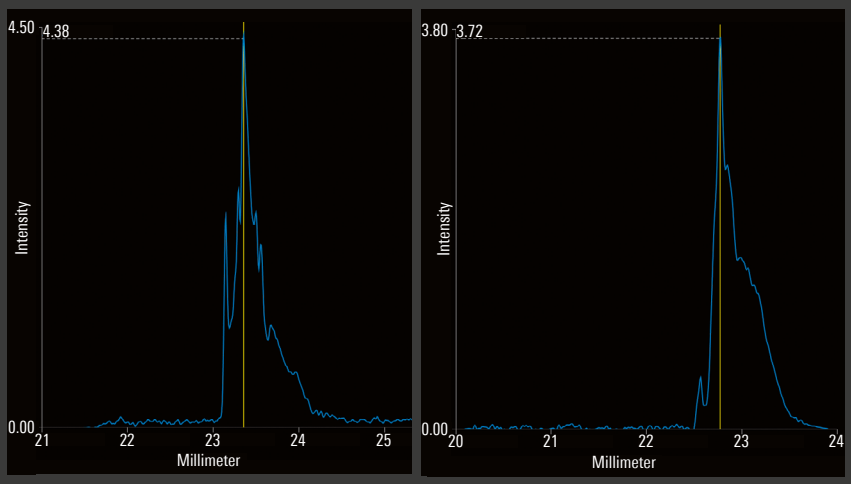

Fig. 23: Axial length graphs of healthy eyes with different appearances and intensities.

EDITING THE AXIAL LENGTH GRAPH

1 Check the retinal peak in the axial length graph. If the automatic peak detection failed or the green vertical line is not aligned with the RPE peak, correct the maximum peak manually by double-clicking the blue graph.
The axial length editor opens.

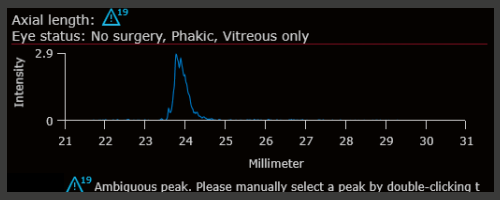

Fig. 24: Automatic peak detection failed.

2 Drag and drop the yellow vertical line to the desired position and confirm by clicking **Save and close**.

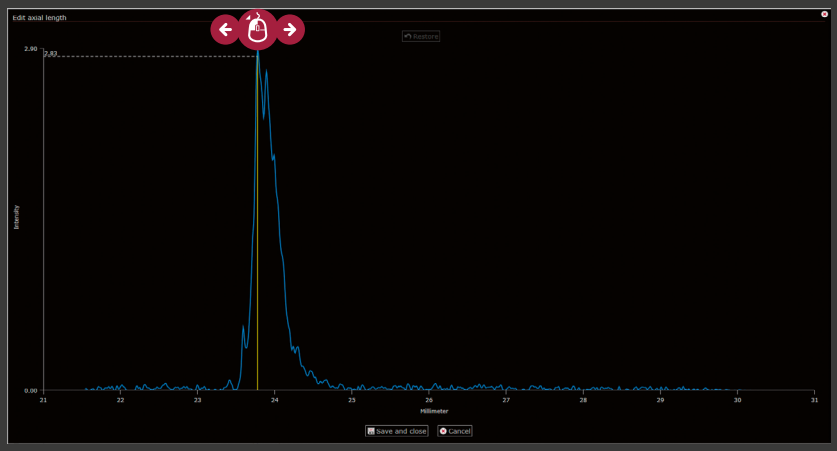

Fig. 25: Axial length editor.

DATA QUALITY

The accuracy of the determined RPE peak/axial length is crucial for accurate IOL power prediction.

2.10 Axial Length Graph Alterations

There are several retinal pathologies that may alter the appearance of the axial length graph depending on the location of the pathology and can have an influence on the results of the eye length measurement.

MANUAL RETINAL PEAK DETECTION

If you are not sure whether the RPE was detected correctly or which peak to mark as RPE in case of failed automatic peak detection, compare the eye length difference with the central retinal layer thickness of the OCT examination as in the examples below.

ELONGATED AXIAL LENGTH GRAPH

An increased distance of the ILM to the RPE may be caused by **edema**, e.g., associated with age-related macular degeneration (AMD), vascular occlusions, diabetic retinopathy or by **retinal traction** in vitreomacular traction or tractional epiretinal membrane.

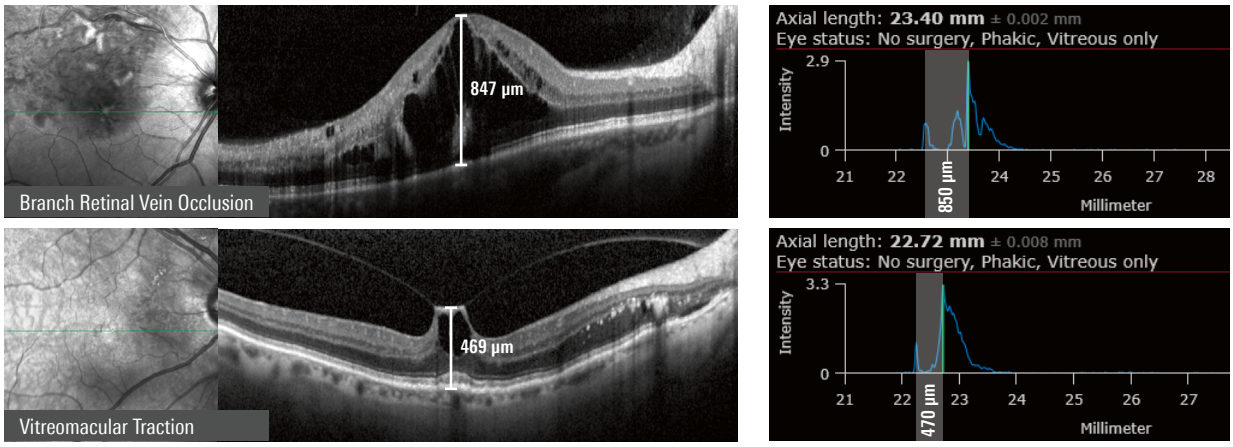

Fig. 26 The graph may be elongated due to edema (top) or traction (bottom).

UNUSUAL CHANGES IN INTENSITIES

An **epiretinal membrane** may cause a high intensity of the first retinal peak due to its high hyperreflectivity.

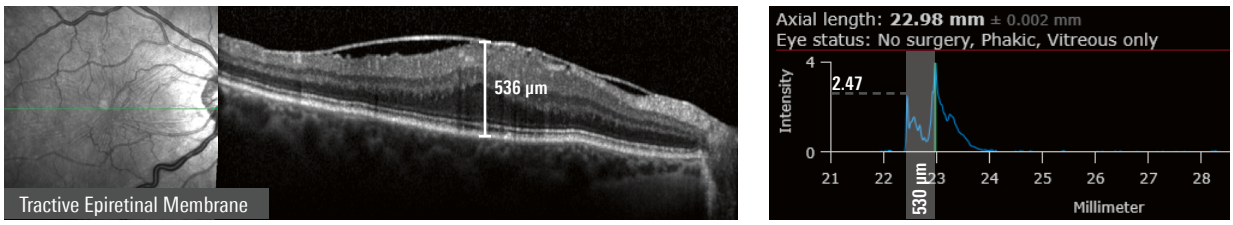

Fig. 27 Epiretinal Membrane causing a high intensity peak of the ILM as well as a lengthening in the ILM-to-RPE distance due to traction.

If the pathology is located in the measuring area, the absence of retinal layers in a **full-thickness macular hole** may cause the first small to moderate ILM peak to be absent and only the highest RPE peak to be evident.

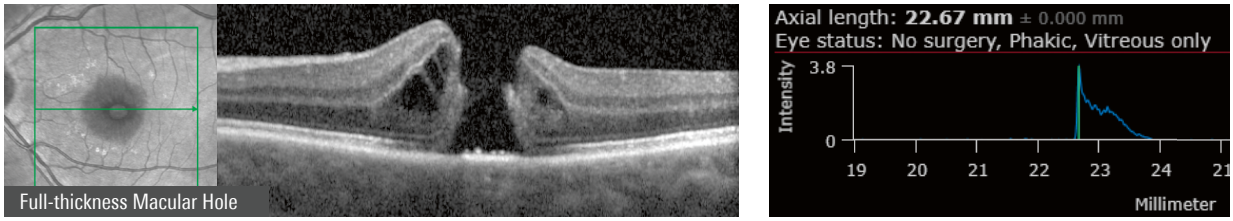

Fig. 28 Missing ILM peak in a full-thickness macular hole. *Image kindly provided by A/Prof. Heriot & Oubada El-Ali, BMedSci, Melbourne, Australia.*

AMBIGUOUS RPE PEAK

If the RPE is pathologically altered by **atrophy, macular neovascularization (MNV), or fibrotic changes** in the area to be measured, automatic detection of the highest RPE peak may fail in some cases.

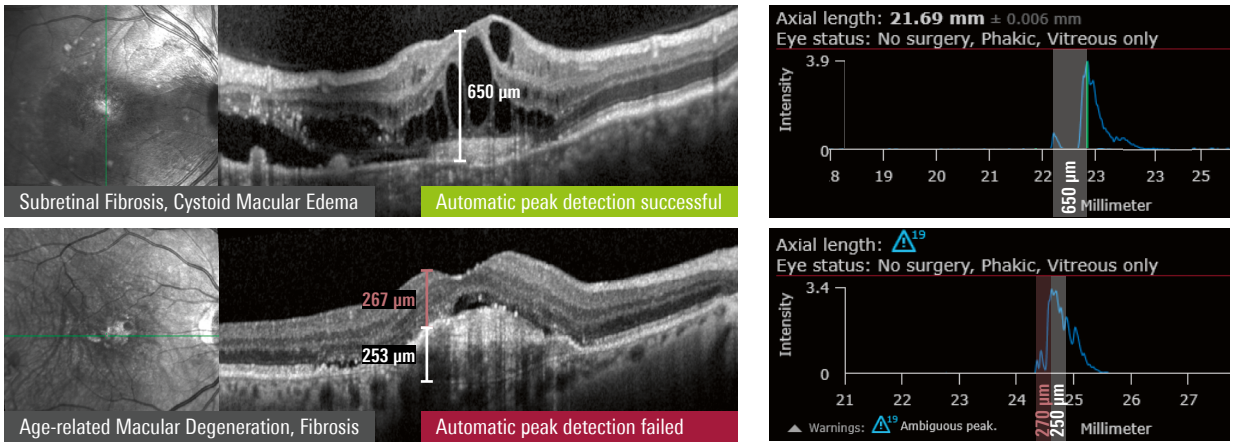

Fig. 29 Successful (top) and failed (below) automatic peak detection due to macular neovascularization and fibrotic changes.

PREOPERATIVE RETINAL EXAMINATION

As part of the preoperative diagnosis, a retinal OCT examination is always recommended to ensure that the axial length measurement has not been affected by pathological changes, e.g., pigment epithelial detachment or macular neovascularization.

In a **pigment epithelial detachment** (PED), the axial length graph may appear inconspicuous because **all** retinal layers are displaced anteriorly due to fluid accumulation **after** the RPE. In this case, the measured eye length would be too short.

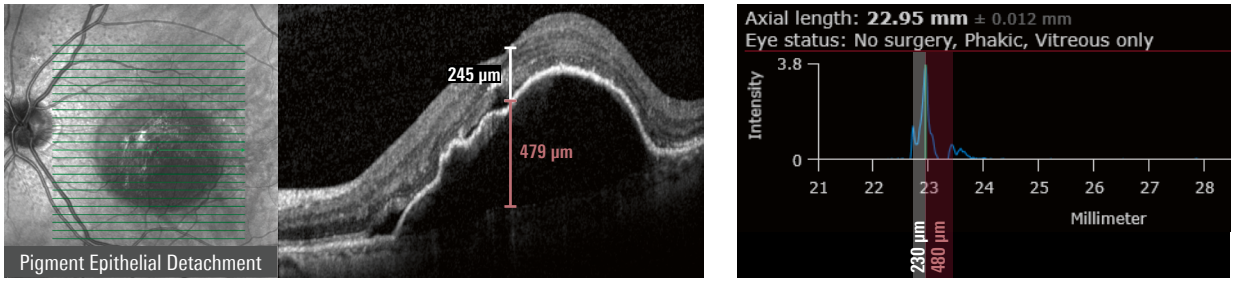

Fig. 30 Inconspicuous looking axial length graph in a pigment epithelial detachment.

3.1 Pretreated Cornea

The cornea accounts for ⅔ of the total refractive power of the eye and is therefore an important structure to be taken into account when predicting the IOL power. The white-to-white (WTW) distance marks the 11–12 mm wide borders of the cornea from the nasal to the temporal limbus. The spherical optical zone is located in the central third. The steeper and thinner center of the cornea becomes flatter and thicker towards the periphery, resulting in an overall negative corneal asphericity. The refractive power depends on the curvature of the anterior and posterior corneal surfaces.

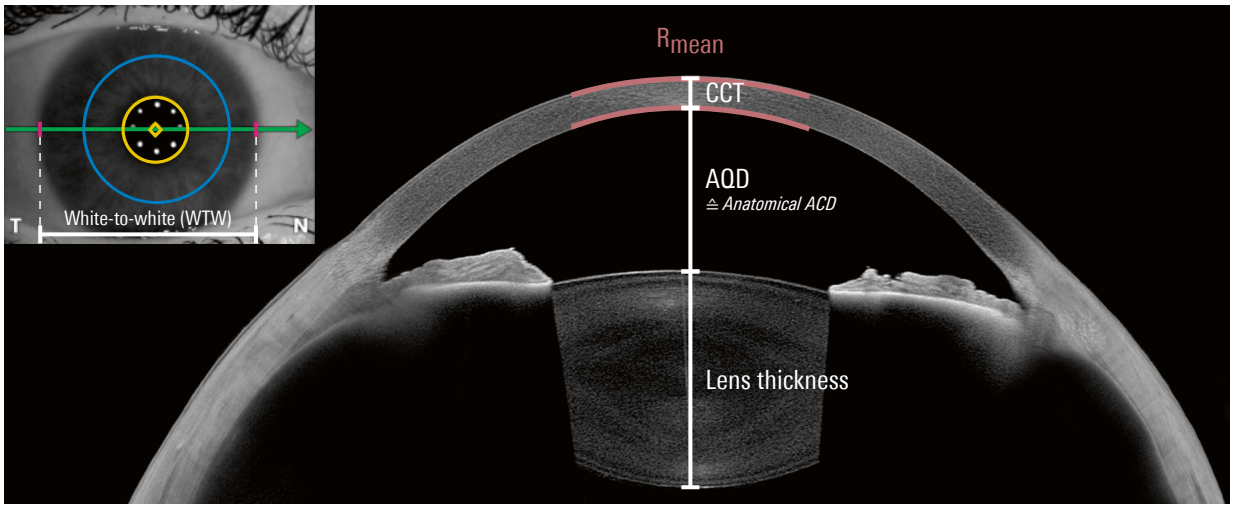

Fig. 31 Anterior segment of the eye. ***CCT*** *Central corneal thickness,* ***AQD*** *Aqueous depth,* ***ACD*** *Anterior chamber depth.*

Most of the commonly used traditional methods for predicting IOL power, such as Haigis or SRK-T, are based on the assumption that the cornea behaves as a thin lens with a constant ratio of the anterior to posterior corneal radius (P/A ratio). When converting corneal anterior surface radii to diopter with ANTERION, the keratometric index of 1.3375 is used. While working with these assumptions is sufficient for normal eyes, it can lead to errors when predicting the IOL power and position in challenging eyes due to deviations in corneal shape.

After laser vision correction, eyes show changes in corneal asphericity and curvature compared to a virgin eye due to the ablation profile correcting myopia or hyperopia. This affects the symmetry and curvature of the anterior corneal radius, the P/A ratio as well as the total refractive power and wavefront of the cornea, especially spherical aberration. The ablation profile differs in size or shape of the ablation and transition zone depending on the procedure.

MYOPIC ABLATION PROFILE

With myopic laser vision correction, the **anterior axial curvature is flattened** by stromal ablation in the central cornea (Fig. 32). Therefore the **P/A ratio decreases** and the **total refractive power is reduced** (Fig. 33). Since biometers only measure corneal radii in the paracentral region (3 mm ring, red circles and dots in fig. 32 and 33) the centrally flatter radius is not taken into account in the measurement. As a result, there is a tendency to **overestimate the corneal radius** and therefore the corneal refractive power.

The application of methods in which corneal curvature (R_{mean})/dioptric power (K_{mean}) is used to estimate the effective lens position may lead to the following errors:

- Underestimation of IOL power
- More anterior IOL position
- Increased risk of hyperopia after IOL implantation

Fig. 32 Schematic illustration of a myopic ablation profile (grey line) and biometry measuring area (red dots).

Furthermore, **higher-order aberrations (HOA), especially spherical aberration, increase**. Depending on the size and/or tilt of the ablation zone, asymmetric HOA may also occur (with significantly higher spherical aberration).

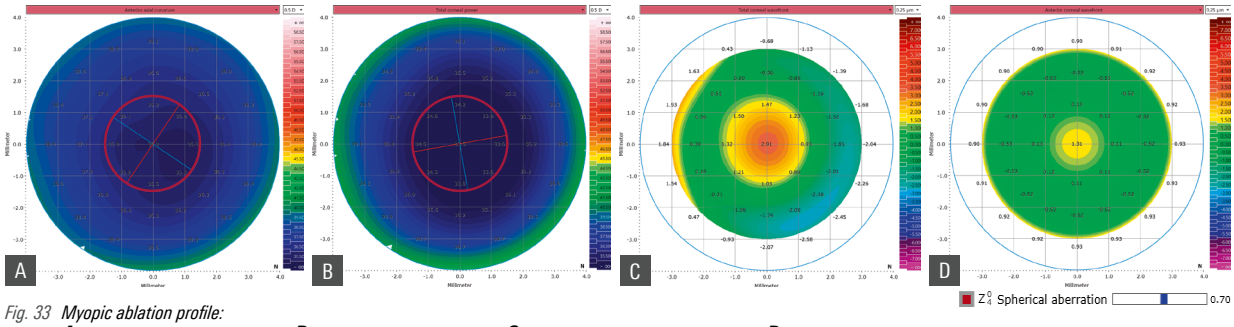

Fig. 33 Myopic ablation profile:
***A** Flatter anterior axial curvature, **B** weaker total corneal power, **C** increased higher order aberrations, **D** higher spherical aberration (0.70 µm).*
Image kindly provided by Damien Gatinel, MD, PhD.

HYPEROPIC ABLATION PROFILE

In hyperopic laser vision correction, the circular stromal ablation in the peripheral cornea causes a **steeper anterior axial curvature** and therefore an **increase in total corneal power**. As the affected region is more likely to be in the peripheral area of biometry measurement (3 mm ring, red circles and dots in fig. 34 and 35), the anterior axial curvature can be assumed to be too flat and thus the refractive power underestimated.

The application of methods in which corneal curvature (R_{mean})/ dioptric power (K_{mean}) is used to estimate the effective lens position may lead to an:

- Overestimation of IOL power
- More posterior IOL position
- Increased risk of myopia after IOL implantation

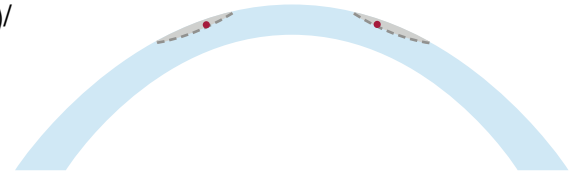

Fig. 34 Schematic illustration of a hyperopic ablation profile (grey line) and biometry measuring area (red dots).

Postoperatively, this leads to a **more negative spherical aberration** and a **decrease in Q-value**. In contrast, the **total HOAs and the RMS of the coma increase** (Fig. 35).[26]

The extent of the change depends on a number of factors, e.g. the chosen procedure, size and/or decentration of the ablation zone.

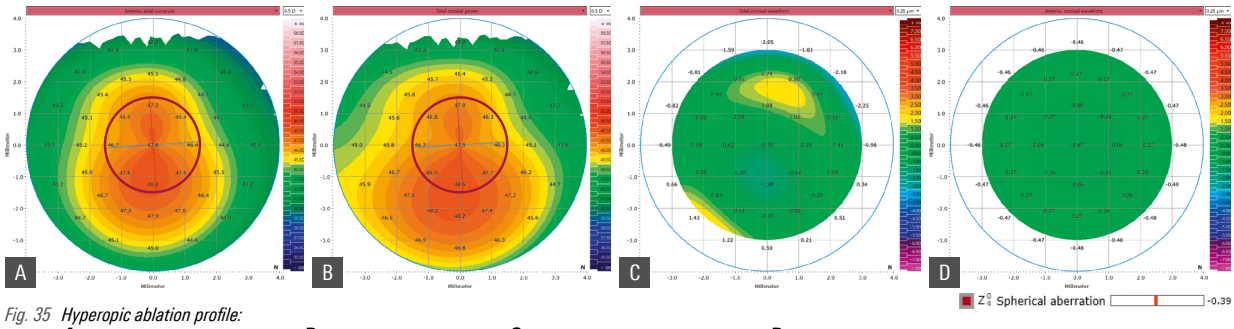

Fig. 35 Hyperopic ablation profile:
***A** Steeper anterior axial curvature, **B** higher total corneal power, **C** increased higher order aberrations, **D** lower spherical aberration (-0.39 µm)*
Image kindly provided by Dr. Cynthia Roberts, PhD & Dr. David Castellano, MD, Columbus, OH, USA.

3.2 Short and Long Eyes

Short eyes with an axial length below 22 mm are usually associated with a steeper cornea and shallower anterior chamber depth. IOL formulas with two variables (axial length and keratometry) also rely on this assumption.

Possible errors in determining the effective lens position (ELP) arise when corneal curvature and anterior chamber depth differ from this assumption.[27] A difference in IOL position in short eyes affects postoperative refraction approx. three times more than in long eyes. Other sources of error may be a shorter distance from IOL to retina and/or a higher refractive power of the IOL required, as they have a higher manufacturing tolerance.[28]

In biometry, a high level of acquisition and data quality should be ensured as measurement errors have a greater impact on short eyes than on normal or long eyes. For example, when predicting the postoperative ACD, a prediction error of 0.25 mm causes an error of 0.1 D for a 30 mm long eye, but 0.5 D for a 20 mm short eye.[29]

*Tab. 1: Measurement errors and resulting refraction errors.[29] **ACD** Anterior chamber depth, **IOL** Intraocular lens.*

VARIABLE	ERROR	REFRACTION ERROR
Corneal radius	1.0 mm	5.7 D
Axial length	1.0 mm	2.7 D
Postop. ACD	1.0 mm	1.5 D
IOL power	1.0 D	0.67 D

In contrast to short eyes, **long eyes with an axial length over 26 mm** tend to be associated with a flatter cornea, thinner lens and deeper anterior chamber depth.[30] If these structures deviate from this assumption, possible errors in the determination of the ELP may arise. However, due to the lower IOL power required (and the resulting lower manufacturing tolerances), the IOL position does not affect the postoperative refraction as much as in the short eye.[28]

3.3 Post Vitrectomy Eyes

Some retinal and/or vitreous diseases require a vitreous replacement surgery, e.g. retinal detachment and tears, especially with proliferative vitreoretinopathy, macular holes, diabetic retinopathies or severe epiretinal membranes.[31] For this purpose, oil, gas or air is inserted into the eye to apply pressure to the posterior pole. As air and gas endotamponades are generally temporary,[32] biometry should be avoided with these eyes.

Silicone oil can often serve as a long-term replacement of the vitreous, but long-term tamponades tend to develop cataract after surgery.[31] Furthermore, the replacement with oil affects the viscosity and the refractive index of the vitreous. Since optical biometers generate the geometric axial length from the optical pathway using a mean refractive index, this can lead to altered axial length values compared to the preoperative length. Therefore, biometry should be performed prior to vitrectomy.

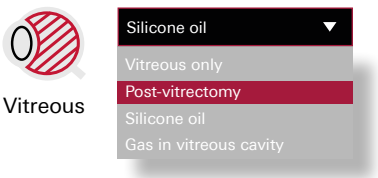

Fig. 36 Eye status of the vitreous.

NO PREOPERATIVE BIOMETRY AVAILABLE

If no preoperative biometry data is available and a examination has to be performed postoperatively, select the eye status **Post-vitrectomy** and predict the IOL power using OKULIX, so that the altered refractive index of the vitreous replacement oil can be entered and thus taken into account.

An axial length value is only available if you select **Vitreous only** or **Post-vitrectomy** as the eye status of the vitreous.

4 Appendix

4.1 Table of Terms and Definitions

ACD	Anterior chamber depth
AMD	Age-related macular degeneration
AQD	Aqueous depth
BFS	Best fit sphere
CCT	Central corneal thickness
ELP	Effective lens position
HOA	Higher-order aberration
ILM	Internal limiting membrane
IOL	Intraocular lens
K	Keratometry
n_{ah}	Refractive index of the aqueous humor
n_c	Refractive index of the cornea
n_k	Keratometric index
OD	Right eye (lat. oculus dexter)
OS	Left eye (lat. oculus sinister)
OU	Both eyes (lat. oculus uterque)
P/A ratio	The ratio of the posterior axial corneal curvature radius to the anterior axial corneal curvature radius
RMS	Root mean square
RMS HOA	Root mean square (RMS) wavefront error of higher-order aberration (HOA)
RPE	Retinal pigment epithelium
TCP	Total corneal power
SimK	Simulated keratometry
WTW	White-to-white

4.2 References

1. KIM KY et al.: Anterior segment characteristics in normal and keratoconus eyes evaluated with a new type of swept-source optical coherence tomography. PLoS One 2022; 17(9):e0274071. DOI: 10.1371/journal.pone.0274071.
2. HERBER R et al.: Agreement and repeatability of corneal tomography in healthy eyes using a new swept-source OCT a rotating Scheimpflug camera and a dual Scheimpflug-Placido system. J Cataract Refract Surg 2022; 48(2):190-198.
3. KIM K et al.: Diagnostic Validation of the Screening Corneal Objective Risk of Ectasia Analyzer Evaluated by Swept Source Optical Coherence Tomography for Keratoconus in an Asian Population. Bioengineering (Basel) 2023; 10(11):1335.
4. The Heidelberg Engineering ANTERION Anterior Segment Cornea and IOL Precision and Agreement Study [data on file].
5. TAÑÁ-RIVERO P et al.: Repeatability of whole-cornea measurements using a new swept-source optical coherence tomographer. Eur J Ophthalmol 2021; 31(4): 1709-1719.
6. ESCOLANO SERRANO J et al.: Intraobserver Repeatability of Tomographic Pachymetric and Anatomical Measurements in Healthy Eyes Using a New Swept-Source Optical Coherence Topographer. Cornea 2022; 41(5):598-603.
7. HERBER R et al.: Comparison of corneal tomography using a novel swept-source optical coherence tomographer and rotating Scheimpflug system in normal and keratoconus eyes: repeatability and agreement analysis. Eye Vis (Lond) 2022; 9(1):19.
8. PÉREZ-BARTOLOMÉ F et al.: Anterior-Segment Swept-Source Ocular Coherence Tomography and Scheimpflug Imaging Agreement for Keratometry and Pupil Measurements in Healthy Eyes. J Clin Med 2021; 10(24):5789.
9. SAAD A et al.: Discrimination between keratoconus forme fruste keratoconus and normal eyes using a novel OCT-based tomographer. J Cataract Refract Surg 2023; 49(11):1092-1097.
10. SCHIANO-LOMORIELLO D et al.: Repeatability of automated measurements by a new anterior segment optical coherence tomographer and biometer and agreement with standard devices. Sci Rep 2021; 11(1):983.
11. CHENG SM et al.: Repeatability of a new swept-source optical coherence tomographer and agreement with other three optical biometers. Graefes Arch Clin Exp Ophthalmol 2022; 260(7): 2271-2281.
12. TAÑÁ-RIVERO P et al.: Agreement between 2 swept-source OCT biometers and a Scheimpflug partial coherence interferometer. J Cataract Refract Surg 2021; 47(4): 488-495.
13. TAÑÁ-RIVERO P et al.: Lens-vault analysis and its correlation with other biometric parameters using swept-source OCT. J Optom 2022; 15(1):88-99.
14. TANA-SANZ P et al.: Agreement of predicted intraocular lens power using swept-source optical coherence tomography and partial coherence interferometry. Expert Rev Med Devices 2021; 18(12): 1219-1234.
15. RUIZ-MESA R et al.: Ocular biometric repeatability using a new high-resolution swept-source optical coherence tomographer.Expert Rev Med Devices 2020; 17(6): 591-597.
16. CHENG SM et al.: Repeatability and Agreement of Two Swept-Source Optical Coherence Tomographers for Anterior Segment Parameter Measurements. J Glaucoma 2022; 31(7): 602-608.
17. XIE X et al.: Age- and refraction-related changes in anterior segment anatomical structures measured by swept-source anterior segment OCT. PLoS One 2020; 15(10):e0240110. DOI: 10.1371/journal.pone.0240110.
18. PARDESHI AA et al.: Intradevice Repeatability and Interdevice Agreement of Ocular Biometric Measurements: A Comparison of Two Swept-Source Anterior Segment OCT Devices. Transl Vis Sci Technol 2020; 9(9): 14.
19. CHAN PP et al.: Anterior chamber angle imaging with swept-source optical coherence tomography: Comparison between CASIAII and ANTERION. Sci Rep 2020; 10(1): 18771.
20. SAVINI G: Posterior Corneal Measurements by 4 Devices. IOL Power Club; November 2023; Palm Springs (not published).
21. PÉREZ-BARTOLOMÉ F et al.: Agreement between anterior segment swept source-OCT and Scheimpflug imaging corneal aberration measurements in healthy eyes. Eur J Ophthalmol 2022; 32(6):3363-3371.
22. YUN JS et al.: Evaluation of angle-to-angle and spur-to-spur using swept source optical coherence tomography in different refractive error. PLoS One 2022; 17(11):e0277703.
23. MONTÉS-MICÓ R et al.: Angle-to-angle and spur-to-spur distance analysis with high-resolution optical coherence tomography. Eye Vis (Lond) 2020; 7:42.
24. MONTÉS-MICÓ R et al.: Assessment of anterior segment measurements using a high-resolution imaging device. Expert Rev Med Devices 2020; 17(9): 969-979.
25. TAÑÁ-RIVERO P et al.: Agreement of white-to-white measurements with swept-source OCT Scheimpflug and color LED devices. Int Ophthalmol 2021; 41(1): 57-65.
26. LIN F et al.: Comparison of visual outcomes and higher-order aberrations between FS-LASIK and SMI-LIKE for moderate to high hyperopia: a 2-year result. Cornea 2022; 10-1097.
27. DE OCA IM et al.: IOL calculations in short, long, and postrefractive eyes. International Ophthalmology Clinics 2016; 56(3): 49-70.
28. HAIGIS W: Preoperative intraocular lens power calculations in problem eyes. Zeitschrift fur Medizinische Physik 2007; 17(1): 45-54.
29. OLSEN T: Calculation of intraocular lens power: a review. Acta Ophthalmologica Scandinavica 2007; 85(5): 472-485.
30. KOTHARI SS et al.: Recent developments in the intraocular lens formulae: An update. Seminars in Ophthalmology 2023; 38(2): 143-150.
31. CHEN Y et al.: Silicone oil in vitreoretinal surgery: indications, complications, new developments and alternative long-term tamponade agents. Acta ophthalmologica 2021; 99(3): 240-250.
32. KANCLERZ P, GRZYBOWSKI A: Complications associated with the use of expandable gases in vitrectomy. Journal of ophthalmology 2018: 8606494.

Headquarters
Heidelberg Engineering GmbH · Max-Jarecki-Str. 8 · 69115 Heidelberg · Germany
Tel. +49 6221 64630 · Fax +49 6221 646362

AUS
Heidelberg Engineering Pty Ltd · Suite E5, 63 Turner Street · Port Melbourne 3207 · Victoria
Tel. +61 396 392 125 · Fax +61 396 392 127

CH
Heidelberg Engineering GmbH · Schulstrasse 161 · 8105 Regensdorf
Tel. +41 44 8887 020 · Fax +41 44 8887 024

FIN
Heidelberg Engineering GmbH · Suomen sivuliike · Fonseenintie 1 · 00370 Helsinki
Tel. +358 505 226 963

UK
Heidelberg Engineering Ltd. · 55 Marlowes · Hemel Hempstead · Hertfordshire HP1 1LE
Tel. +44 1442 502 330 · Fax +44 1442 242 386

US
Heidelberg Engineering Inc. · 10 Forge Parkway · Franklin, MA 02038
Tel. +1 508 530 7900 · Fax +1 5085307901

www.HeidelbergEngineering.com